MULTIMODE BACKWARD WHIRL MOTION IN ROTOR-STATOR CONTACT

Oliver Alber*[1], Nicklas Norrick[1], Benjamin Siegl[1]

[1]Institute for Structural Dynamics, TU Darmstadt
alber@sdy.tu-darmstadt.de
{norrick,siegl}@sdy.tu-darmstadt.de

Keywords: Rotor-Stator Contact, Backward Whirl, Multimode, Rub, MDOF.

Abstract. *In this work multimode backward whirl motion patterns during rotor-stator interaction are investigated. Additional degrees of freedom are taken into account by analysis of a system with many degrees of freedom for rotor and for stator. A multifrequent approach can be extended to this type of system in order to calculate all possible backward whirl motion patterns. Therefore a synchronous as well as a negative asynchronous frequency component is used. An analytical approach to solve the resulting equations is described. The stability of the predicted backward whirl motion patterns is checked by* POINCARÉ *maps obtained from the steady-state simulation data of the nonlinear system. The influence of system parameters on the existence and stability of various backward whirl motion patterns is investigated for two examples.*

LIST OF SYMBOLS

A   center of contact ring
$\boldsymbol{B}$ damping matrix
D damping ratio
d diameter
F force
i complex unit
$\boldsymbol{K}$ stiffness matrix
k stiffness coefficient
$\boldsymbol{l}$ contact position vector
$\boldsymbol{M}$ mass matrix
M   number DOF rotor, mass center of disk
m mass
N   number DOF stator,
    normal component
$\widehat{\boldsymbol{q}}$ modeshape
R   shaft center
$\boldsymbol{r}$ complex displacement vector
r complex displacement
S   center of the stator
s average nominal gap
t time
δ instantaneous minimal gap

$\boldsymbol{\varepsilon}$ vector of radial excentricity
ε radial excentricity
μ_F friction coefficient
φ rotation angle of rotor
ψ contact point angle
Ψ backward whirl frequency
Ω rotor speed
ω natural frequency
$\dot{()}$ time derivative $(=\frac{d()}{dt})$
$\widetilde{()}$ modal coefficient
$|()|$ amplitude
$\langle () \rangle$ FOEPPL-Symbol,
    $(= ()$ for $() \geq 0, = 0$ else$)$
$()_C$ contact (position)
$()_F$ friction
$()_{roll}$ rolling
$()_R$ rotor
$()_{RS}$ rotor and stator coupled
$()_S$ stator
$()^T$ transposed
$()_\Psi$ backward whirl
$()_\Omega$ synchronous

1 INTRODUCTION

When a rotor contacts a non-rotating part like its housing or an auxiliary bearing, the system becomes nonlinear and various motion patterns are possible. Besides motions with a dominant synchronous frequency component (for example synchronous, forward whirl, sideband, sub-, superharmonic and chaotic motions) backward whirl motion patterns, or in literature (e.g. [1]) often referred to as *dry whip*, may occur. This motion pattern generally contains a small synchronous frequency component as well as a dominant negative asynchronous frequency component. It exhibits large vibration amplitudes combined with huge contact forces which might lead to severe damage of the whole rotor-stator system. In a simple description a JEFFCOTT rotor can contact a flexibly mounted rigid stator. For this model Black [2] described possible backward whirl motion using an approach with an asynchronous frequency component Ψ only. Rotor and stator deflection $(r_R(t), r_S(t))$ as well as the contact force $F_C(t)$ are expressed by

$$r_R(t) = \widehat{r}_R e^{i\Psi t}; \qquad r_S(t) = \widehat{r}_S e^{i\Psi t}; \qquad F_C(t) = \widehat{F}_C e^{i\Psi t}. \tag{1}$$

This approach is widely known in literature and has been used in many further studies (e.g. Bartha [3], Crandall [4]). Lingener [5] performed experimental studies confirming the theoretical assumptions. Ehehalt et al. [6] took into account a synchronous as well as an asynchronous frequency component to describe backward whirl motion. This approach is more general than (1). Childs [1] extended the simple model and investigated backward whirl motion with a multimode rotor and a single-mode stator model. He concludes that for multimode rotor-stator contact many backward whirl motions are possible. Multiple coexisting backward whirl

motions have also been identified experimentally [7]. For a slightly different model considering a JEFFCOTT rotor with an additional degree of freedom for the inclination angle and therefore significant gyroscopic effects Siegl et al. [8] also showed the occurence of multiple backward whirl motions. However, the reason and the condition for stability and coexistence of multiple backward whirl motions during rotor-stator contact are not clear yet.

2 MODELING ASSUMPTIONS

Rotor-stator contact with many degrees of freedom can be described using the model from [9] and [10], which is shown in Figure 1.   The rotor consists of a massless, linear-elastic
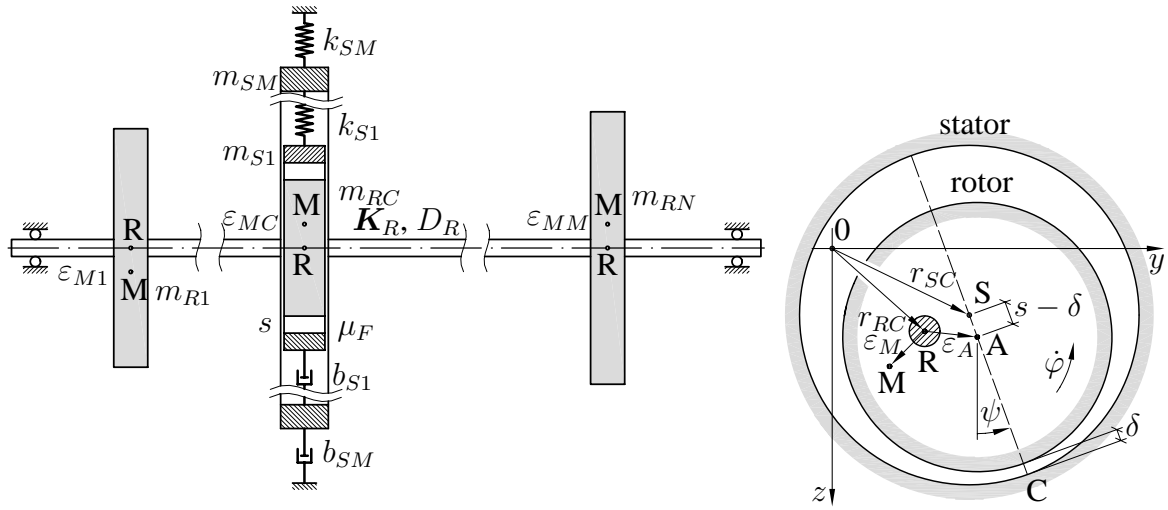

Figure 1: MDOF system for rotor-stator contact and kinematics of the contact plane (from [6]).

shaft and N mass disks. These mass disks are fixed at the shaft with a complex excentricity ε_{Mn}, described by the excentricity vector $\boldsymbol{\varepsilon}_M$. The stiffness matrix $\boldsymbol{K}_R$ of the rotor is isotropic. Gyroscopic effects are neglected in this work. The rotor is able to contact the stator at position C with cylindrical contact surfaces at a distance s. The stator system consists of M flexibly mounted rigid rings with an isotropic stiffness matrix $\boldsymbol{K}_S$. For rotor and stator only deflections in the yz plane are considered. Modal damping described by the modal damping ratios D_R and D_S for rotor and stator is taken into account. From [11] the damping matrices $\boldsymbol{B}_R$ and $\boldsymbol{B}_S$ can be calculated by

$$\boldsymbol{B} = \boldsymbol{M}\Big(\sum_{n=1}^{N} \frac{2D_n\omega_n}{\widetilde{m}_n} \widehat{\boldsymbol{q}}_n \widehat{\boldsymbol{q}}_n^T\Big)\boldsymbol{M}. \tag{2}$$

$\boldsymbol{M}$ is the mass matrix, $\widehat{\boldsymbol{q}}_n$ the n-th mode shape and ω_n the n-th natural frequency of rotor or stator. Modal coefficients are denoted with a tilde: $\widetilde{m}_{Rn} = \widehat{\boldsymbol{q}}_{Rn}^T \boldsymbol{M}_R \widehat{\boldsymbol{q}}_{Rn}$ for example is the n-th modal mass of the rotor. The equations of motion for the rotor and stator deflection vectors $\boldsymbol{r}_R$ and $\boldsymbol{r}_S$ using complex notation for steady-state rotation (Ω=const.) are

$$\boldsymbol{M}_R \ddot{\boldsymbol{r}}_R + \boldsymbol{B}_R \dot{\boldsymbol{r}}_R + \boldsymbol{K}_R \boldsymbol{r}_R = \boldsymbol{M}_R \boldsymbol{\varepsilon}_M \Omega^2 e^{i\Omega t} - \boldsymbol{l}_R F_C \tag{3}$$

for the rotor and

$$\boldsymbol{M}_S \ddot{\boldsymbol{r}}_S + \boldsymbol{B}_S \dot{\boldsymbol{r}}_S + \boldsymbol{K}_S \boldsymbol{r}_S = \boldsymbol{l}_S F_C \tag{4}$$

for the stator. The contacting coordinates for rotor and stator are described by the contact position vectors l_R and l_S, which contain the value one for the contacting coordinates and otherwise zero. If rotor and stator are moving independently from each other or if contact is established is determined by the instantaneous minimal gap δ between rotor and stator. Size and orientation of the instantaneous minimal gap δ are obtained by the kinematic relation

$$l_R^T r_R + \varepsilon_A e^{i\Omega t} - l_S^T r_S = (s-\delta)e^{i\psi} \tag{5}$$

to

$$\psi = \arg\left\{l_R^T r_R + \varepsilon_A e^{i\Omega t} - l_S^T r_S\right\} \qquad \text{and} \qquad \delta = s - (l_R^T r_R + \varepsilon_A e^{i\Omega t} - l_S^T r_S)e^{-i\psi}. \tag{6}$$

Contact is established if the instantaneous minimal gap δ is smaller or equal to zero. In the case of contact a normal force F_{CN} and a friction force $F_{CT} = i\mu_F F_{CN}$ result, for which the COULOMB friction law is used. The complex contact force is $F_C = (1+i\mu_F)F_{CN}$. The direction of the normal component of the distance between rotor and stator is identical to the direction of the normal contact force F_{CN}:

$$e^{i\psi} = \frac{l_R^T r_R + \varepsilon_A e^{i\Omega t} - l_S^T r_S}{|l_R^T r_R + \varepsilon_A e^{i\Omega t} - l_S^T r_S|} = \frac{F_{CN}}{|F_{CN}|} = \frac{1-i\mu_F}{\sqrt{1+\mu_F^2}}\frac{F_C}{|F_C|} \tag{7}$$

In general it has to be differed between two important contact descriptions: The kinematic condition $\delta = 0$ for contact is resulting in

$$l_R^T r_R + \varepsilon_A e^{i\Omega t} - l_S^T r_S = s\frac{1-i\mu_F}{\sqrt{1+\mu_F^2}}\frac{F_C}{|F_C|}. \tag{8}$$

This relation is based upon rigid contact surfaces and for contact reduces the degrees of freedoms by one. For numerical simulations the pseudolinear contact model by [6]

$$F_C = (1+i\mu_F)F_{CN} = (1+i\mu_F)\left\langle -k_C\delta - b_C\langle\dot{\delta}\rangle\right\rangle\langle-\delta\rangle^0 e^{i\psi}, \tag{9}$$

with $\langle\rangle$ as an extended switch function, is more suitable. This model avoids tensile forces and for sufficient contact stiffness k_C delivers similar results as (8).

These expressions are only valid if the tangential velocity of the rotor at the contact position C is greater than the tangential velocity of the stator and the rotor is always sliding in positive direction of $\varphi = \Omega t$. If the shaft center of the rotor is propagating backwards with a constant frequency Ψ this results in the condition [3]:

$$-\frac{\dot{\Psi}}{\Omega} < \frac{d_R}{2s} \tag{10}$$

According to Ehehalt in most systems the average nominal gap s is small compared to the rotor contact surface diameter d_R, so condition (10) is violated only for very small rotation speed Ω.

A widely used definition for *backward whirl* motion is a rotor rolling in the stator. This is only the case if the tangential velocities of rotor and stator are equal, which leads to a backward roll frequency Ψ_{roll} proportional to the rotating speed Ω [3]:

$$\Psi_{roll} = -\Omega\frac{d_R}{s} \tag{11}$$

Due to experimental observations in [5] and [7] which explicitly observe sliding of the rotor in the stator, this special case shall not be studied in this work.

3 ANALYTICAL APPROACH FOR MULTIMODE BACKWARD WHIRL

The equations of motion for rotor (3) and stator (4) with many degrees of freedom as well as the kinematic contact condition (8) can be analyzed with respect to possible backward whirl motions. As shown in many publications (e.g. [6], [7]) the frequency spectrum of a backward whirl motion pattern with continuous contact between rotor and stator generally exhibits a synchronous frequency component Ω as well as a negative asynchronous frequency component Ψ. Therefore a multifrequent approach similar to [6]

$$\boldsymbol{r}_R(t) = \widehat{\boldsymbol{r}}_{R\Omega} e^{i\Omega t} + \widehat{\boldsymbol{r}}_{R\Psi} e^{i\Psi t} \tag{12}$$

$$\boldsymbol{r}_S(t) = \widehat{\boldsymbol{r}}_{S\Omega} e^{i\Omega t} + \widehat{\boldsymbol{r}}_{S\Psi} e^{i\Psi t} \tag{13}$$

$$F_C(t) = \widehat{F}_{C\Omega} e^{i\Omega t} + \widehat{F}_{C\Psi} e^{i\Psi t} \tag{14}$$

for the rotor deflection $\boldsymbol{r}_R(t)$, stator deflection $\boldsymbol{r}_S(t)$ and contact force $F_C(t)$ is used. Separation of the frequency components results in a set of equations for the synchronous frequency Ω

$$(-\Omega^2 \boldsymbol{M}_R + i\Omega \boldsymbol{B}_R + \boldsymbol{K}_R)\widehat{\boldsymbol{r}}_{R\Omega} = \Omega^2 \boldsymbol{M}_R \boldsymbol{\varepsilon}_S - \boldsymbol{l}_R \widehat{F}_{C\Omega} \tag{15}$$

$$(-\Omega^2 \boldsymbol{M}_S + i\Omega \boldsymbol{B}_S + \boldsymbol{K}_S)\widehat{\boldsymbol{r}}_{S\Omega} = \boldsymbol{l}_S \widehat{F}_{C\Omega} \tag{16}$$

$$(\boldsymbol{l}_R^T \widehat{\boldsymbol{r}}_{R\Omega} - \boldsymbol{l}_S^T \widehat{\boldsymbol{r}}_{S\Omega}) = s\frac{1 - i\mu_F}{\sqrt{1 + \mu_F^2}} \frac{\widehat{F}_{C\Omega}}{|\widehat{F}_{C\Psi}|} \tag{17}$$

as well as a set of equations for the asynchronous frequency Ψ:

$$(-\Psi^2 \boldsymbol{M}_R + i\Psi \boldsymbol{B}_R + \boldsymbol{K}_R)\widehat{\boldsymbol{r}}_{R\Psi} = -\boldsymbol{l}_R \widehat{F}_{C\Psi} \tag{18}$$

$$(-\Psi^2 \boldsymbol{M}_S + i\Psi \boldsymbol{B}_S + \boldsymbol{K}_S)\widehat{\boldsymbol{r}}_{S\Psi} = \boldsymbol{l}_S \widehat{F}_{C\Psi} \tag{19}$$

$$(\boldsymbol{l}_R^T \widehat{\boldsymbol{r}}_{R\Psi} - \boldsymbol{l}_S^T \widehat{\boldsymbol{r}}_{S\Psi}) = s\frac{1 - i\mu_F}{\sqrt{1 + \mu_F^2}} \frac{\widehat{F}_{C\Psi}}{|\widehat{F}_{C\Psi}|} \tag{20}$$

It has been shown that the asynchronous frequency components are dominant compared to the synchronous frequency components. As a result of this $|F_{C\Omega} + F_{C\Psi}|$ is replaced by $|F_{C\Psi}|$ in the kinematic relations (17) and (20). Furthermore ε_A is neglected.

Solving for the asynchronous frequency components, if $\widehat{\boldsymbol{r}}_{R\Psi}$ and $\widehat{\boldsymbol{r}}_{S\Psi}$ from equation (18) and (19) are inserted into equation (20) one obtains

$$|\widehat{F}_{C\Psi}| = s\frac{1 - i\mu_F}{\sqrt{1 + \mu_F^2}} \frac{1}{-\boldsymbol{l}_R^T(-\Psi^2 \boldsymbol{M}_R + i\Psi \boldsymbol{B}_R + \boldsymbol{K}_R)^{-1}\boldsymbol{l}_R - \cdots} \frac{1}{\cdots \boldsymbol{l}_S^T(-\Psi^2 \boldsymbol{M}_S + i\Psi \boldsymbol{B}_S + \boldsymbol{K}_S)^{-1}\boldsymbol{l}_S} . \tag{21}$$

As the contact force amplitude $|\widehat{F}_{C\Psi}|$ is always real, the imaginary part of the right hand side of equation (21) has to be zero:

$$\Im\{|\widehat{F}_{C\Psi}|\} \overset{!}{=} 0 \tag{22}$$

From this additional relation the unknown asynchronous frequency component Ψ can be calculated. If compared to results with a simulation model using the contact condition (9), the contact
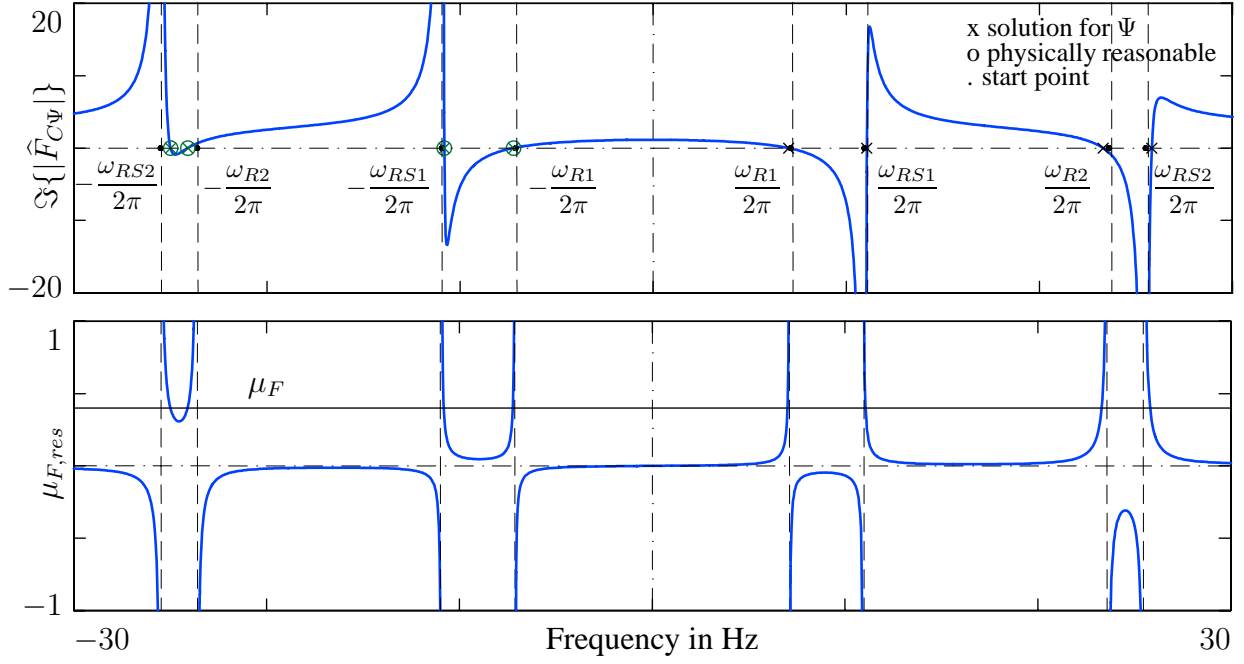
5

Figure 2: Imaginary part $\Im\{|\widehat{F}_{C\Psi}|\}$ and resulting friction coefficient $\mu_{F,res}$ vs. frequency for example 1.

stiffness k_C has to be considered. The right hand side of equation (21) contains the complex transfer functions at the contact position of rotor $H_{R,CC}(\Psi)$ and stator $H_{S,CC}(\Psi)$:

$$H_{R,CC}(\Psi) = \boldsymbol{l}_R^T(-\Psi^2\boldsymbol{M}_R+i\Psi\boldsymbol{B}_R+\boldsymbol{K}_R)^{-1}\boldsymbol{l}_R \tag{23}$$

$$H_{S,CC}(\Psi) = \boldsymbol{l}_S^T(-\Psi^2\boldsymbol{M}_S+i\Psi\boldsymbol{B}_S+\boldsymbol{K}_S)^{-1}\boldsymbol{l}_S \tag{24}$$

Equation (21) also can be transformed to the equation used in [1] and [2] for the simple system:

$$\Big(H_{R,CC}(\Psi)+H_{S,CC}(\Psi)\Big)|\widehat{F}_{C\Psi}| = -s\frac{1-i\mu_F}{\sqrt{1+\mu_F^2}} \tag{25}$$

The amplitudes of the asynchronous rotor and stator deflection $\widehat{\boldsymbol{r}}_{R\Psi}$ and $\widehat{\boldsymbol{r}}_{S\Psi}$ are calculated with equations (18) and (19). Combining (15), (16) and (17) the synchronous contact force component can be expressed by

$$\widehat{F}_{C\Omega} = \cfrac{\boldsymbol{l}_R^T(-\Omega^2\boldsymbol{M}_R+i\Omega\boldsymbol{B}_R+\boldsymbol{K}_R)^{-1}\Omega^2\boldsymbol{M}_R\boldsymbol{\varepsilon}_S}{s\dfrac{1-i\mu_F}{\sqrt{1+\mu_F^2}}\dfrac{1}{|\widehat{F}_{C\Psi}|}+\boldsymbol{l}_R^T(-\Omega^2\boldsymbol{M}_R+i\Omega\boldsymbol{B}_R+\boldsymbol{K}_R)^{-1}\boldsymbol{l}_R\cdots} \atop {\cdots+\boldsymbol{l}_S^T(-\Omega^2\boldsymbol{M}_S+i\Omega\boldsymbol{B}_S+\boldsymbol{K}_S)^{-1}\boldsymbol{l}_S} \tag{26}$$

4 PREDICTED BACKWARD WHIRL FREQUENCY

An analytical solution of equation (22) is not suitable, as the order of Ψ becomes very big even for simple systems with two rotor and two stator degrees of freedom. As a matter of this equation (22) is solved numerically using a Bisection Search Algorithm to find the roots for the asynchronous frequency Ψ. If the system damping is weak, the poles of this equation are located in the vicinity of $\pm\omega_{Rn}$, $\pm\omega_{Sm}$ and $\pm\omega_{RSi}$, so the natural frequencies and coupled natural frequencies of rotor and stator are used as starting points for the algorithm. As an

alternative approach Black [2] solves equation (25) graphically by calculating the resulting friction coefficient

$$\mu_{F,res} = -\tan\Big(\arg\{H_{R,CC}(\Psi) + H_{S,CC}(\Psi)\}\Big). \tag{27}$$

The intersection points of function (27) with the actual friction coefficient μ_F are the possible asynchronous frequencies Ψ_i. Black also states that for each U-shaped section of $\mu_{F,res}$ the solutions with lower frequencies are stable. Figure 2 shows the imaginary part of the asynchronous contact force amplitude $\Im\{|\widehat{F}_{C\Psi}|\}$ for a system with small damping (example 1 in table 1). In this case the roots are located close to the coupled natural frequencies ω_{RSi} and the rotor natural frequencies ω_{Ri}. The start points are marked as points and possible asynchronous frequencies Ψ_i obtained by solving equation (22) are displayed by x. The algorithm is capable of finding the roots of $\Im\{|\widehat{F}_{C\Psi}|\}$ reliably. Equal to Ehehalt [6] all Ψ_i are checked regarding physical reasonability (green and marked by O) using the following three criteria:

- $|r_{R\Psi}| > s$: The rotor deflection at the contact position shall be greater than the gap size

- $|F_{C\Psi}| > 0$: There shall be no tensile forces

- $\Im\{\Psi\} = 0$: The obtained asynchronous frequencies have to be real

Only negative asynchronous frequencies Ψ_i deliver results that are physically reasonable. In the lower part the resulting friction coefficient $\mu_{F,res}$ of equation (27) is displayed. Both methods deliver the same results for Ψ_i and can be used instead of each other.

		example 1	example 2
friction coefficient	μ_F	0.4	0.2
rotor damping ratio	D_R in %	0.6	0.6
stator damping ratio	D_S in %	2	1.1
gap size	s in mm	1.3	1.3
mass excentricity	ε_M in mm	$[0.1 \quad 0.1e^{-i\pi/2}]^T$	$[0.1 \quad 0.1e^{-i\pi/2}]^T$
natural frequency			
rotor 1st mode	$\omega_R/2\pi$ in Hz	7.1	9.2
rotor 2nd mode	$\omega_R/2\pi$ in Hz	23.6	32.9
stator 1st mode	$\omega_R/2\pi$ in Hz	176.8	28.5
stator 2nd mode	$\omega_R/2\pi$ in Hz	832.5	252.1
rotor and stator coupled			
1st mode	$\omega_{RS1}/2\pi$ in Hz	10.9	13.5
2nd mode	$\omega_{RS2}/2\pi$ in Hz	25.5	32.5
3rd mode	$\omega_{RS3}/2\pi$ in Hz	811.63	161

Table 1: System parameters used in the examples.

These semi-analytical solutions allow a study of the influence of different parameters onto possible backward whirl motions. In Figure 3 different system parameters for example 1 are varied. The damping ratio for rotor D_R and stator D_S influence the presence of backward whirl motions. Above a critical limit for D no backward whirl motion is possible. These
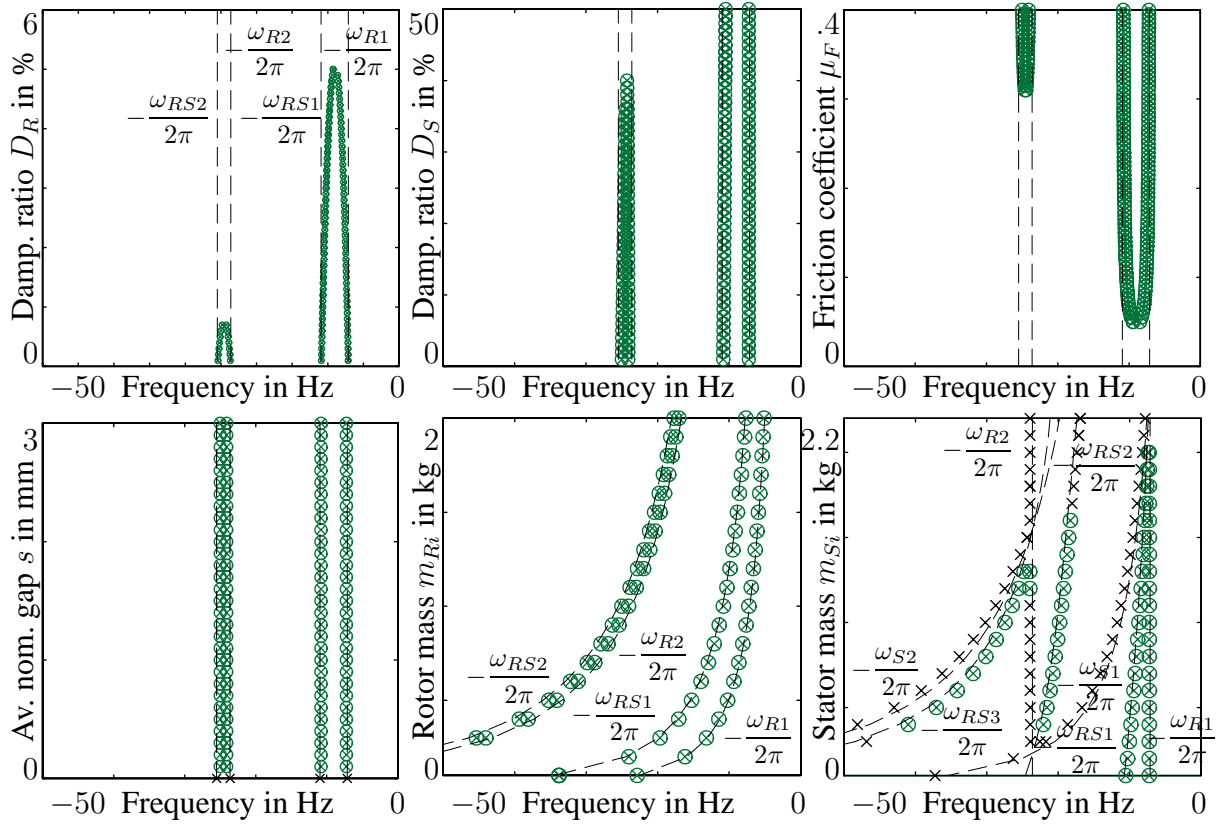
Figure 3: Asynchronous backward whirl frequency Ψ for variation of different parameters for example 1.

results agree with the statement from Black [2], Bartha [3] and Ehehalt [6] for simple systems, that the risk for backward whirl motion decays with increasing system damping. The critical damping ratio at which backward whirl motion vanishes is higher for the first set of solutions with $\Psi \approx -\omega_{RS1}$ than for the second set of solutions at $\Psi \approx -\omega_{RS2}$. Above a rotor damping ratio of $D_R = 1\%$ no backward whirl motion for $\Psi \approx -\omega_{RS2}$ exists. For the chosen system with stator natural frequencies above the rotor natural frequencies backward whirl motion with high-frequency Ψ is more difficult to establish than backward whirl motion with low-frequency Ψ. If the damping ratio is decreased further, the solutions for possible Ψ are located at $-\omega_{Rn}$ and $-\omega_{RSi}$. This correlates with the observation from Ehehalt [6], that for an undamped JEFFCOTT rotor contacting a massless stator the solutions for the negative backward whirl frequencies Ψ_i are equal to $\pm\omega_R$ and $\pm\omega_{RS}$. Backward whirl motion is only possible above a certain critical friction coefficient μ_F. Same as for the damping, the limitations for the friction coefficient of the second set of solutions are more strict than for the first set. Hence with $\mu_F \leq 0.3$ no backward whirl motion for $\Psi \approx -\omega_{RS2}$ is possible. A change of the average nominal gap s has no influence on possible backward whirl motions. If the relation between the rotor and stator natural frequencies are changed (variation of m_{Ri} or m_{Si}) it can be seen that close to the intersection of natural frequencies of rotor and stator a motion suddenly can become physically reasonable. For the simple case Black [2] and Bartha [3] state that Ψ is located between the rotor natural frequency ω_R and the coupled natural frequency of rotor and stator ω_{RS}. This statement is only valid if the stator natural frequencies are higher than those of the rotor. If rotor and stator natural frequencies cross, this behavior changes.
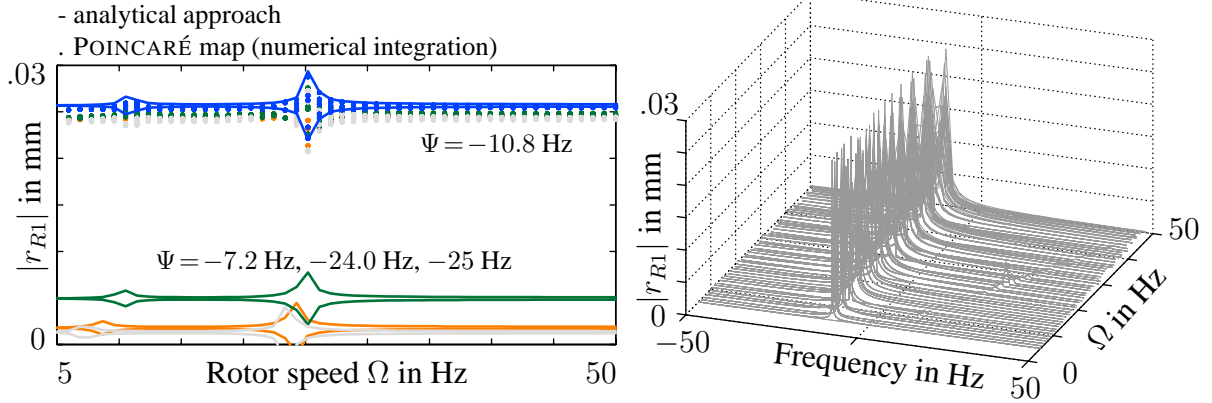
Figure 4: Bifurcation diagram and frequency spectrum for example 1.
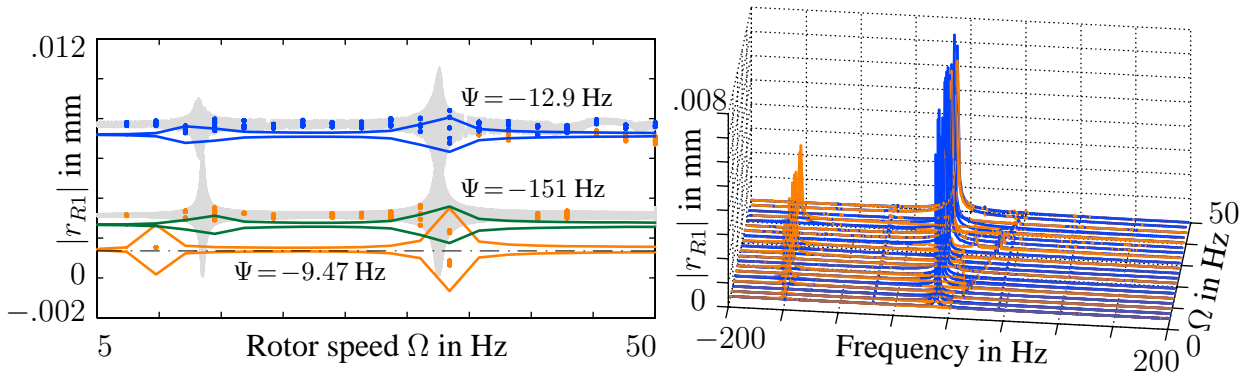

Figure 5: Bifurcation diagram and frequency spectrum for example 2.

5 STABILITY INVESTIGATIONS

Even if a possible solution of equation (22) is physically reasonable, it can be unstable. So the physically reasonable motions have to be checked regarding stability. Therefore the calculated motions for each reasonable solution of equation (22) are used as initial conditions for the numerical integration of equations (3), (4) and (9). A stationary numerical simulation is performed and a POINCARÉ map is generated by sampling the rotor motion for a fixed rotation angle. A bifurcation diagram based on this data is created for bifurcation analysis of the rotor speed Ω. As a control variable the rotor deflection amplitude of the contacting disk $|r_{R1}|$ is chosen. All results for example 1 (dots) are displayed together with the analytically calculated solutions (lines) in Figure 4. For the presented case only the backward whirl motion with $\Psi = -10.8$ Hz is stable, which can be seen in the bifurcation diagram as well as in the spectrum. For this motion the rotor deflection amplitudes are bigger than for the other solutions. The asynchronous frequency Ψ of this motion is very close to the negative first coupled natural frequency $-\omega_{RS1} = -10.9$ Hz. If other solutions are used as initial conditions for numerical integration of the nonlinear system of equations, again a motion with $\Psi = -10.8$ Hz is established, showing that other predicted backward whirl motions are not stable. The calculated semi-analytical solution delivers a good prediction for the stable motion state. In addition example 2 is shown in figure 5. For this example two backward whirl motions are stable, but the predicted amplitudes are not matching exactly to the simulation results. For the motion with $\Psi = -12.9$ Hz this is due to a partial contact between rotor and stator. For the motion with $\Psi = -151$ Hz the asynchronous component is close to the size of the synchronous component. Thus for both cases the idealized assumptions are violated.

9

6 CONCLUSIONS

A multifrequent approach is used to solve the nonlinear equations in rotor-stator contact with many degrees of freedom for backward whirl motion. As an alternative to the solution of Black [2], a semi-analytical approach is developed. For example systems with 2 DOF for rotor and for stator possible backward whirl motions are investigated for various system parameters. The multimode systems exhibit properties that are already known for the simple system with a JEFFCOTT rotor and a single DOF stator. An increased occurrence of low-frequency backward whirl motion is experienced. Stability analysis of the predicted motions is performed by a POINCARÉ map based on stationary numerical simulations. For the first example only one backward whirl motion is stable. The predicted motion matches perfectly to the numerical results. The stability investigation shows, that the backward whirl motion, which is located in the vicinity of the negative first coupled natural frequency ($\Psi \approx -\omega_{RS1}$), is most likely to occur. For a different example two stable backward whirl motions, but also partial contact are present. The results are object to be validated experimentally.

REFERENCES

[1] D.W. Childs and A. Bhattacharya, Prediction of Dry-Friction Whirl and Whip Between a Rotor and a Stator. *Journal of Vibration and Acoustics*, **127**, 594–603, 2005.

[2] H. F. Black, Interaction of a whirling rotor with a vibrating stator across a clearance annulus. *Journal Mechanical Engineering Science*, **10**, 1–12, 1968.

[3] A. Bartha, *Dry Friction Backward Whirl of Rotors*. Dissertation, Swiss Federal Institute of Technology, Zrich, 2000.

[4] S. Crandall, From Whirl to Whip in Rotordynamics. *3rd Int. Conf. for Rotordynamics*, IFTOMM, Lyon, France, 19–26, 1990.

[5] A. Lingener, Experimental Investigation of Reverse Whirl of a Flexible Rotor. *3rd Int. Conf. for Rotordynamics*, IFTOMM, Lyon, France, 13–18, 1990.

[6] U. Ehehalt, D. Hochlenert and R. Markert, An Analytical Description of Backward Whirl Caused by Rotor-Stator-Contact. *10th International Symposium on Transport Phenomena and Dynamics of Rotating Machinery*, ISROMAC, Honolulu, Hawaii, 1–10, 2004.

[7] J. Wilkes, D. Childs, B. Dyck and S. Phillips, The Numerical and Experimental Characteristics of Multimode Dry-Friction Whip and Whirl. *Journal of Engineering for Gas Turbines and Power*, **132**, 052503-1–052503-9, 2010.

[8] B. Siegl, N. Norrick and R. Markert, Theoretical Investigations on Rotor-Stator-Contact of Rotors with Distinctive Gyroscopic Effects. M. A. Savi eds. *XV International Symposium on Dynamic Problems of Mechanics*, DINAME, Buzios, Brazil, 1–9, 2013.

[9] O. Alber, Rotor Stator Interaction with Many Degrees of Freedom. *83. Jahrestagung GAMM*, Darmstadt, Germany, 1–2, 2013.

[10] G. Wegener, *Elastische Fanglager zur Amplitudenbegrenzung elastischer Rotoren*. Fortschr.-Ber. VDI Reihe 11 Nr. 290, Dsseldorf, 2000.

[11] R. Markert, *Strukturdynamik (Maschinendynamik I)*. Lecture Notes, TU Darmstadt, 2006.